ACS Sustainable Chemistry & Engineering

pubs.acs.org/journal/ascecg

Research Article

Structural Study of a Eutectic Solvent Reveals Hydrophobic Segregation and Lack of Hydrogen Bonding between the Components

Matteo Busato,* Giorgia Mannucci, Valerio Di Lisio, Andrea Martinelli, Alessandra Del Giudice, Alessandro Tofoni, Chiara Dal Bosco, Valentina Migliorati, Alessandra Gentili, and Paola D'Angelo*

Cite This: *ACS Sustainable Chem. Eng.* 2022, 10, 6337−6345

Read Online

ACCESS | Metrics & More | Article Recommendations | Supporting Information

ABSTRACT: An in-depth study of the hydrophobic eutectic solvent formed by butylated hydroxytoluene (BHT) and L-menthol (MEN) in a 1:3 molar ratio has been carried out using an integrated approach that combines differential scanning calorimetry (DSC), attenuated total reflection Fourier transform infrared (ATR-FTIR) spectroscopy, small- and wide-angle X-ray scattering (SWAXS), and molecular dynamics (MD) simulations. The obtained data have been step-by-step compared to those collected on the eutectic formed by 3,5-di-*tert*-butyltoluene (TBT) and MEN in the same molar ratio, where TBT is analogous to the BHT without the hydroxyl group. The DSC characterization showed comparable results between the two systems, evidencing that the hydroxyl group of the BHT has little or no impact on the thermal behavior of the BHT:MEN eutectic. Both the FTIR and MD results agree in finding that no hydrogen bond (H-bond) interactions are played by the BHT because of the high steric hindrance suffered by its hydroxyl group so that the only established H-bonds are those between MEN molecules. The incompatibility between the components in terms of H-bonds formation results in hydrophobic segregation promoting the MEN−MEN interactions, which are even more intense than in the pure compound. The three-dimensional arrangement between the components showed a remarkable degree of structural order among the alkyl functional groups, suggesting that the apolar−apolar attraction might be the driving force of the eutectic formation. This picture is translated into the establishment of an intermediate-range organization in solution, as evidenced by the SWAXS data. The overall impact of this study is that of pushing a little bit further the definition of these eutectics, indicated until now as extensively H-bonded systems.

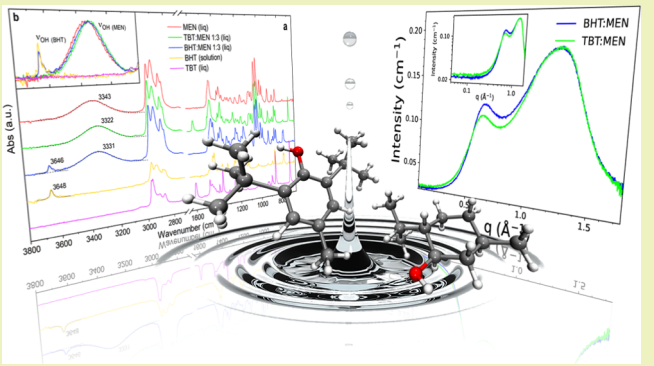

KEYWORDS: *hydrophobic deep eutectic solvents, menthol, butylated hydroxytoluene, differential scanning calorimetry, FTIR spectroscopy, X-ray scattering, molecular dynamics*

INTRODUCTION

The formulation of innovative solvents meeting the requirements of Green Chemistry has certainly become one of the major challenges of academic and industrial research. In this framework, a new class of designer solvents has recently emerged: deep eutectic solvents (DESs).[1] A DES is formed by the judicious combination of a hydrogen bond (H-bond) donor and an acceptor, solid starting materials that melt if put in contact at precise molar ratios. As a result, a liquid mixture is obtained with a melting point (MP) that is not only lower than those of the pure constituents but also lower than the one predicted by assuming a thermodynamic ideal behavior of the liquid phase.[2] The driving force of such a phenomenon has been long debated and seems to rely on the strong and extensive H-bond network that is established between the components so that the species in solution are packed in a manner that maximizes these interactions.[3−9] Besides intrinsic qualities such as easy preparation, no need of purification, and tunable physical−chemical properties, DESs often show other interesting features like negligible vapor pressure, nonflammability, high conductivity, and low toxicity.[10] For these reasons, they are frequently indicated as a more sustainable alternative to traditional solvents for several applications.[11,12]

Even if many efforts have been made so far to find a comprehensive division of DESs into classes, the compositional heterogeneity of these solvents makes this a daunting task. At present, the most efficient classification is that provided by

Received: February 15, 2022
Revised: April 20, 2022
Published: May 2, 2022

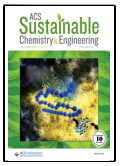

Abbott et al.,[11] who initially divided the DESs into four categories depending on their constituents:

Type I - quaternary ammonium + metal chloride salts;
Type II - quaternary ammonium + metal chloride hydrate salts;
Type III - quaternary ammonium salt + H-bond donor;
Type IV - metal chloride hydrate salt + H-bond donor.

Here, it can be observed that the majority of DESs are based on at least one ionic component, and dominated by strong H-bonding compounds. However, the ongoing research on these solvents has very recently led to the introduction of a new class named "type V".[13] At variance with the previous categories, type V DESs are formed solely by neutral molecular constituents, often consisting of phenolic compounds. As a subclass of type V DESs, hydrophobic DESs (HDESs) have been proposed for the first time in 2015 and represent the latest frontier in the research on these solvents.[14,15] The peculiarity of HDESs is their immiscibility with water, guaranteed by the low water solubility of their components, very often based on terpenoids like thymol and menthol.[13,15−17] As a consequence of their hydrophobicity, they possess significant advantages over common hydrophilic DESs. For example, their ability to form biphasic systems with water makes them more suitable for liquid−liquid extractions and microextractions, allowing the removal of target compounds such as biomolecules,[15] pesticides,[18] medicinal components,[19] volatile fatty acids,[14] metal ions,[20−23] and often outperforming the industrial standards. Further employments of HDESs embrace a wide applicative horizon, among which their use as electrolytes in solar cells,[24] CO_2 capturing agents,[25] additives for coatings,[26] and catalytic media[27] is a long but not conclusive list.

Here, we present a study on a eutectic mixture formed by butylated hydroxytoluene (BHT) and L-menthol (MEN) blended in a 1:3 molar ratio (hereafter called "BHT:MEN"). This eutectic has been very recently developed and has shown outstanding results in liquid−liquid microextractions of pesticides and fat-soluble micronutrients on food samples,[18,28] besides an intrinsic eco-friendly nature provided by its components. In fact, menthol has become a popular constituent of many HDESs because of its availability from natural sources and eco-friendliness, while BHT is known for its antioxidant properties.[29] We have to specify that this mixture has been previously indicated as an ideal eutectic due to the proximity of its experimental MP to the eutectic one.[28] However, likewise their classification, also the definition of the qualities needed to provide a proper DES is still cumbersome, in particular how much the MP depression must be "deep". Such a debate is beyond the scope of the present study; therefore, the umbrella terminology "eutectic" will be used herein to address the studied systems.

Particular emphasis has been put on the structural arrangement in solution to unveil the interactions established among the components. This urgency arises from the observation that the formation of H-bonds by the BHT seems to be dramatically impeded because of the high steric hindrance suffered by its hydroxyl group (Figure 1). The present investigation is therefore addressed to understand if this is the case and, if so, which are the favorable interactions allowing the eutectic formation. To this purpose, a combined approach including differential scanning calorimetry (DSC), attenuated total reflection Fourier transform infrared (ATR-FTIR) spectroscopy, small- and wide-angle X-ray scattering (SWAXS), and molecular dynamics (MD) simulations has been employed. As a comparative term to the BHT:MEN system, the mixture formed by 3,5-di-*tert*-butyltoluene (TBT, Figure 1) and MEN in the same molar ratio ("TBT:MEN") has been also studied. TBT is analogous to the BHT without the hydroxyl group so that the comparison between the two systems will allow us to better understand the involvement of the various constituents in the eutectic formation and in the global structural arrangement in solution.

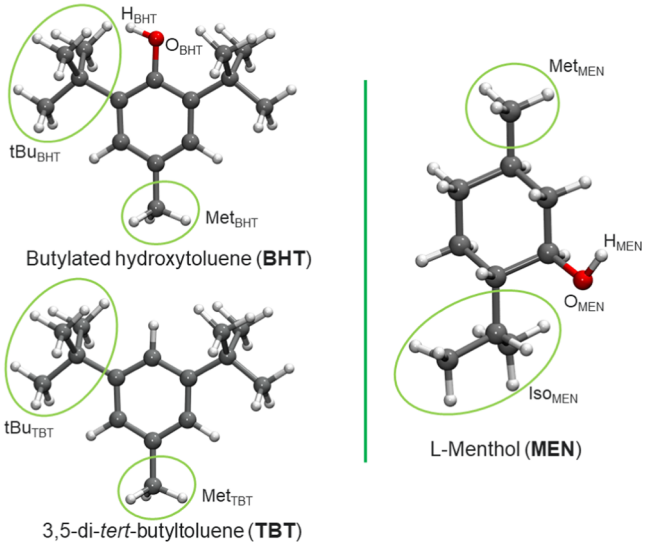

Figure 1. Butylated hydroxytoluene (BHT), 3,5-di-*tert*-butyltoluene (TBT), and L-menthol (MEN) molecular structures within the employed nomenclature for atoms and functional groups.

MATERIALS AND METHODS

Chemicals and Sample Preparation. BHT (food grade, ≥99 %), TBT (95%), and MEN (natural source, food grade, ≥99%) were purchased from Merck (Milan, Italy). The BHT:MEN and TBT:MEN eutectics were prepared by mixing the components at the desired molar ratio in a glass test tube. The samples were then heated at 323 K in a water bath under magnetic stirring, even if the melting has been observed to occur also upon mere contact between the components. As a result, two colorless viscous liquids were obtained, and for both mixtures, a 0.902 g cm^{-3} density was calculated by weighting 1 mL of sample in a volumetric flask. Note that the MPs of the eutectic mixtures were determined to be slightly above room temperature (*vide infra*); therefore, sample storage under these conditions was observed to induce a crystallization process. However, the kinetics of this process is low enough to carry out sample manipulation and analysis on the supercooled liquid phase for a reasonable amount of time.

Differential Scanning Calorimetry. The DSC thermograms of the BHT:MEN and TBT:MEN eutectics were acquired with a Mettler Toledo DSC 822e differential calorimeter (Mettler Toledo, Greifensee, Switzerland), equipped with a ceramic FRS5 sensor and a liquid nitrogen cooler. A sample quantity of about 5 mg was sealed in a 40 μL aluminum pan. For the eutectic samples, the DSC program consisted of a first cooling step at −10 K min^{-1} from 323 to 173 K, followed by a heating ramp from 173 to 323 K at 10 K min^{-1}. The thermal properties of TBT were analyzed by a heating scan from 273 to 353 K at 10 K min^{-1}. During the measurements, the furnace was purged with dry nitrogen with a flow rate of 30 mL min^{-1}. All of the measurements were carried out in duplicate, and the errors were calculated as the semidifferences of the two results.

ATR-FTIR Spectroscopy. Infrared spectra were collected in ATR mode with a Nicolet 6700 spectrometer (Thermo Scientific, Waltham) equipped with a Specac Golden Diamond ATR accessory. Absorbance spectra were acquired at room temperature in the 4000−

https://doi.org/10.1021/acssuschemeng.2c00920
ACS Sustainable Chem. Eng. 2022, 10, 6337−6345

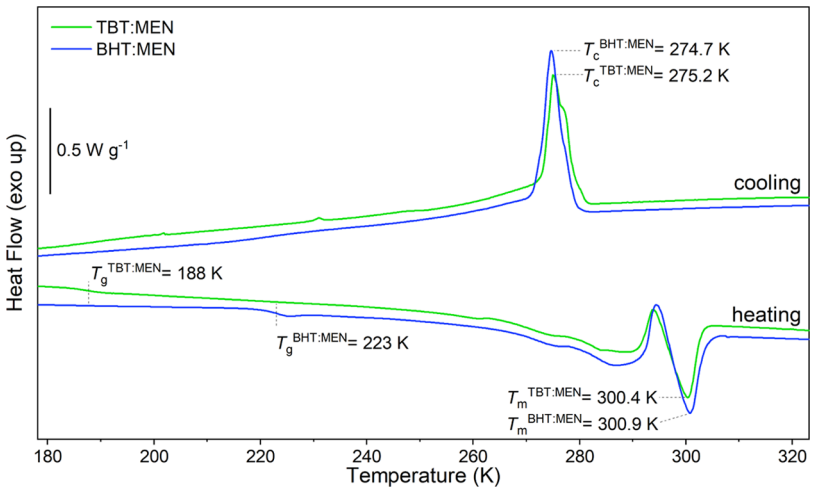

Figure 2. Selected DSC traces of the BHT:MEN (blue line) and TBT:MEN (green line) eutectics recorded at 10 K min^{-1} cooling/heating rate. The crystallization temperature (T_c), glass-transition temperature (T_g), and melting temperature (T_m) are highlighted.

650 cm^{-1} range, by co-adding 200 scans at 4 cm^{-1} resolution. The spectra of MEN, TBT, TBT:MEN, and BHT:MEN were acquired in the liquid form. For this purpose, the pure components MEN and TBT were melted directly on the ATR crystal at about 323 K with a heat gun and cooled at room temperature. In this way, the samples were observed to persist in the supercooled liquid state for several minutes before the crystallization, allowing for data collection. As regards the BHT component, ATR-FTIR data were acquired on a 20% w/v solution of the compound in *n*-heptane. The spectrum of BHT was then obtained by properly subtracting the solvent contribution. The bands connected with the O-H stretching vibrational mode of the hydroxyl groups (ν_{OH}) in the 3800−3000 cm^{-1} region were fitted using a Gaussian profile to obtain the maximum values.

Molecular Dynamics Simulations. Classical MD simulations have been carried out on the BHT:MEN and TBT:MEN systems. Cubic boxes were built with ∼50 Å side lengths and a number of species chosen to reproduce the experimental density of 0.902 g cm^{-3}. Details about the system's composition are reported in Table S1. Structures and interactions of the BHT and TBT molecules were represented with the all-atom optimized potentials for liquid simulations (OPLS-AA) force field,[30] while for the MEN, the OPLS-compatible parameters developed by Jasik et al. were employed.[31] The electrostatic interactions were represented by the Coulomb potential with fixed charges, while for the van der Waals (vdW) part, the Lennard-Jones potential was employed with mixed terms constructed with the Lorentz−Berthelot combining rules. A cutoff radius of 12 Å was applied for all nonbonded interactions, while long-range electrostatic forces were taken into account with the particle mesh Ewald method.[32,33]

Initial configurations were built by randomizing the atomic positions with the PACKMOL package,[34] then each system was equilibrated under NVT conditions following a heating ramp up to 500 K, staying at high temperature for 2 ns, and gradually cooling down to 308 K. High-temperature equilibrations were previously observed to be recommendable for viscous systems like DESs and ionic liquids.[4,35−40] The final production runs for data collection were performed under NVT conditions at 308 K for 50 ns, being this temperature just above the determined MPs of the two eutectics (*vide infra*). The temperature was controlled by coupling the systems to a Nose−Hoover thermostat with a relaxation constant of 0.5 ps, while the equations of motion were integrated by means of the leap-frog algorithm with a 1 fs time step and coordinates were saved every 100 steps. Stretching vibrations involving hydrogen atoms were constrained with the LINCS algorithm.[41] To have a comparison with the pure component, a box of liquid MEN (Table S1) was simulated at 353 K for 50 ns with the same protocol. Also, the BHT:MEN system was simulated at 353 K to carry out a structural comparison at the same temperature. Note that this protocol has been necessary to simulate the liquid state of MEN, while also the BHT:MEN system had to be simulated at the same temperature to provide a correct comparison between the two systems, due to the well-known temperature-induced spreading effect on pair distributions.[42] The experimental density of the pure compound at 353 K (0.877 g cm^{-3})[43] was used to build the MEN system, while the density of the BHT:MEN mixture at 353 K was estimated with a 10 ns NPT run employing the Parrinello−Rahman barostat with a coupling constant of 1.0 ps and resulted to be 0.892 g cm^{-3}.

Simulations were performed with the Gromacs 2020.2 program,[44] while the VMD 1.9.3 software[45] was used for trajectories visualization and the TRAVIS code for the analysis.[46]

SWAXS Measurements. X-ray scattering measurements were performed at the SAXSLab Sapienza with a Xeuss 2.0 Q-Xoom system (Xenocs SAS, Grenoble, France), equipped with a micro-focus Genix 3D X-ray source (λ = 1.542 Å) and a two-dimensional Pilatus3 R 300 K detector that can be placed at variable distances from the sample (Dectris Ltd., Baden, Switzerland). Calibration of the scattering vector q range, where $q = (4\pi \sin\theta)/\lambda$, with 2θ being the scattering angle, was performed with a silver behenate standard. The beam size was defined through the two-pinhole collimation system equipped with scatterless slits to be 0.5 mm × 0.5 mm. Measurements with two different sample−detector distances were performed so that the overall explored q region was 0.02−1.70 Å^{-1}. The BHT:MEN and TBT:MEN eutectics were loaded into vacuum-tight quartz capillary cells and placed within the thermalized holder at a reduced pressure (≈0.2 mbar). Measurements were carried out at 308 K to ensure that the samples were in the liquid state. The two-dimensional scattering patterns were subtracted for the dark counts, and then masked, azimuthally averaged, and normalized for transmitted beam intensity, exposure time, and subtended solid angle *per* pixel, using the FoxTrot software developed at SOLEIL. The one-dimensional intensity *vs* q profiles were then subtracted for the empty capillary contribution and put in absolute scale units (cm^{-1}) by dividing the capillary cell thickness estimated by calibration with water. The different angular ranges were merged using the SAXSutilities tool.[47]

RESULTS AND DISCUSSION

DSC Characterization. The selected DSC traces of the BHT:MEN and TBT:MEN eutectics are shown in Figure 2. During cooling from the liquid state at 323 K down to 173 K, both mixtures exhibit a sharp crystallization occurring at a temperature of T_c = 275 ± 1 K for BHT:MEN and 275 ± 2 K for TBT:MEN, respectively. In the subsequent heating ramp,

https://doi.org/10.1021/acssuschemeng.2c00920
ACS Sustainable Chem. Eng. 2022, 10, 6337−6345

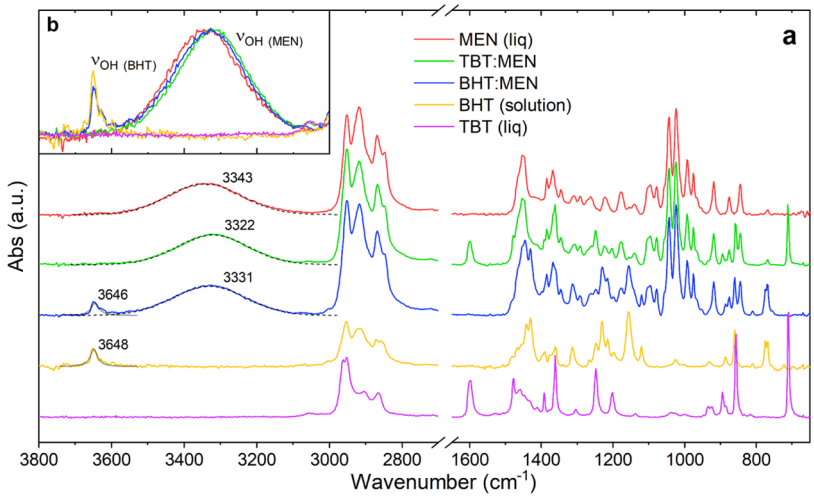

Figure 3. (a) ATR-FTIR spectra of the BHT:MEN (blue) and TBT:MEN (green) eutectics, and of the MEN (red), BHT (orange), and TBT (purple) constituents. The peaks connected with the ν_{OH} contributions of BHT and MEN have been fitted with Gaussian curves reported in dashed gray to find the position of the maxima. (b) The 3800−3000 cm^{-1} region is reported in the inset as superimposed spectra to emphasize the comparison of the MEN and BHT ν_{OH} bands.

the glass-to-liquid transition occurs at low temperatures as a step in the heat flow at T_g = 223 ± 2 and 188 ± 1 K for BHT:MEN and TBT:MEN, respectively. Note that the T_g values can be determined with less precision because of the broader shape of the features connected with these transitions. Sequentially, the pre-melting appears as a broad convolution of several endothermic peaks between about 260 and 290 K, followed up by the final melting at T_m = 300.9 ± 0.5 K for BHT:MEN and 300.4 ± 0.2 K for TBT:MEN. These values are coherent with the predicted MP of the ideal eutectic mixtures (295 K), computed by considering the α-crystalline fraction of MEN,[13] and are, of course, significantly lower than those of the pure components BHT (343 K) and MEN (316 K),[28] as well as TBT (307 ± 1 K, Figure S1). At this point, it is worth emphasizing that the BHT component differs from the TBT one for the presence of a hydroxyl group. At least at first glance, it should be therefore legit to predict a different thermal behavior between the BHT:MEN and TBT:MEN systems, as a reflection on a macroscopic property due to the different chemical nature of the constituents. However, the two eutectics show great similarities in the collected DSC traces, this result being even more remarkable if we take into account the difference in the MP of the BHT and TBT starting compounds.[28,48] Such an evidence can therefore be taken as a direct proof of the lack of participation of the BHT hydroxyl group to the thermal behavior of the BHT:MEN mixture, and opens the question about its involvement even in the interactions at the molecular level and in the structural arrangement occurring in solution.

Study of the H-Bond Interactions: ATR-FTIR Analysis. ATR-FTIR spectroscopy has been employed to investigate the intermolecular interactions occurring in solution and, in particular, the formation of H-bonds between the components through the study of the ν_{OH} band, which is known to be correlated with the H-bond strength.[5,6,49] For this purpose, FTIR spectra were acquired for the BHT:MEN and TBT:MEN mixtures and compared with those collected on the single constituents MEN, BHT, and TBT. The obtained data are shown in Figure 3a. The lower-wavenumber region (1600−650 cm^{-1}) of the absorption spectra of the mixtures results from a superimposition of the spectral features of the pure compounds so that no useful information about the interaction between the components can be drawn from this region. Differently, the 3800−3000 cm^{-1} region is dominated by the ν_{OH} contributions (Figure 3b). The O−H stretching of the BHT solution occurs at relatively high wavenumbers (3648 cm^{-1}), this feature being characteristic of weak or negligible H-bonds. Note that these data have been collected on an *n*-heptane solution and that the solvent is not expected to take part in the formation of H-bonds due to its apolarity. Conversely, the ν_{OH} of liquid MEN is connected with a broad band centered at 3343 cm^{-1} after fitting with a Gaussian curve, highlighting the formation of strong H-bonds between the MEN molecules in the pure compound. As regards the absorption spectrum of the BHT:MEN mixture, it can be observed that the ν_{OH} of the BHT remains basically unchanged with respect to the pure component, strongly suggesting that this species poorly participates in the formation of H-bonds also in the eutectic solvent. In addition, the ν_{OH} band of MEN remains qualitatively very similar to that of the pure compound, provided a slight but detectable redshift from 3343 to 3331 cm^{-1}, which is even more marked in the absorption spectrum of the TBT:MEN mixture (3322 cm^{-1}) and thus follows the MEN > BHT:MEN > TBT:MEN trend. The whole result suggests that the MEN molecules in the BHT:MEN mixture retain a degree of H-bonding that is even slightly stronger than that of liquid MEN. This circumstance may arise from the fact that, when MEN is mixed with BHT, the low propensity of the latter compound to form H-bonds results in a steric exclusion toward the MEN component that is able to promote the formation of MEN−MEN H-bonds. This sort of hydrophobic segregation is even more pronounced in the TBT:MEN eutectic, as a consequence of the even lower affinity between the components because of the absence of a hydroxyl group in TBT.

Study of the H-Bond Interactions: MD Results. To obtain a confirmation of the FTIR results and an atomistic description of the interactions occurring in solution, MD simulations were carried out on the BHT:MEN and TBT:MEN systems. First, site−site radial distribution functions $g(r)$'s have been calculated for all of the possible intermolecular H−O distributions in the BHT:MEN to verify

https://doi.org/10.1021/acssuschemeng.2c00920
ACS Sustainable Chem. Eng. 2022, 10, 6337−6345

which are the actual H-bonds formed in solution. The obtained $g(r)$'s are shown in Figure 4a. Here, it can be observed that one

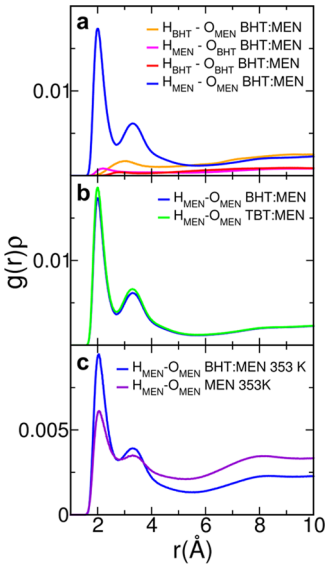

Figure 4. Radial distribution functions multiplied by the numerical densities of the observed atoms, $g(r)\rho$'s, calculated from the MD simulations at 308 K for the intermolecular H-O distributions in the BHT:MEN system (a) and for the H_{MEN}-O_{MEN} distribution in the BHT:MEN and TBT:MEN systems (b), and in the MEN and BHT:MEN systems at 353 K (c). The atom names are employed according to the nomenclature reported in Figure 1.

function is particularly overwhelming with respect to the others, namely, the H_{MEN}-O_{MEN} one relatable to the H-bond between the MEN molecules. Integration of this $g(r)$ up to the first minimum at 2.69 Å provides a coordination number N of 0.53, while the first peak maximum position of 2.01 Å is in line with those typically observed for strong H-bonds.[50] However, the bond distance is not the only criterion to define if an H−O distribution might be connected to a real H-bond, and the analysis of the bond angle formed between the donor and the acceptor is often mandatory.[50] For this reason, we also computed the combined distribution function (CDF) between the intermolecular H_{MEN}-O_{MEN} $g(r)$ and the related bond angle (Figure S2). The obtained map shows a high probability spot around 180°, thus confirming the H_{MEN}-O_{MEN} distribution as a strong H-bond. As regards the remaining H-O $g(r)$'s computed for the BHT:MEN eutectic, both the H_{BHT}-O_{MEN} and the H_{MEN}-O_{BHT} distributions show poorly structured peaks of negligible intensity, and the same is true for the H_{BHT}-O_{BHT} one (Figure 4a). In particular, the coordination numbers obtained for the H_{MEN}-O_{BHT} and H_{BHT}-O_{BHT} $g(r)$'s are less than 0.1, while the H_{BHT}-O_{MEN} distribution is connected with a broad peak centered at 3.00 Å. This result confirms that almost no H-bond interactions between the BHT and MEN constituents occur, as well as between the BHT molecules, and the only relevant H-bonds established in solution are those between MEN molecules, in agreement with the FTIR analysis. This evidence is quite surprising since at least on paper the H_{BHT}-O_{MEN} interaction should be the most important one in the eutectic formation, due to the resonance effects of the BHT molecule. In fact, the electron lone pair of the oxygen atom in BHT can be delocalized through the aromatic ring (Figure S3), making the hydroxyl group more positive and the H_{BHT} atom a better donor. On the other hand, the MEN molecule possesses no aromaticity so that when BHT and MEN are mixed, the preferable interaction should be established between the H_{BHT} donor and the O_{MEN} acceptor. This circumstance has been already employed to explain the eutectic formation in the archetypal type V HDES formed by thymol and MEN.[13] Differently, in our case, the obtained results unambiguously show that the high steric hindrance suffered by the BHT hydroxyl group is able to overwhelm these electrostatic effects and to prevent the formation of H-bonds by the BHT component.

To have further confirmation of the FTIR data, the H_{MEN}-O_{MEN} $g(r)$ has been computed also for the TBT:MEN system and compared to that obtained for the BHT:MEN one (Figure 4b). As a result, the two $g(r)$'s are nearly superimposable, confirming that the MEN molecules retain a similar degree of H-bonding after mixing with either BHT or TBT. In addition, even if the shapes of the two curves are very similar, the H_{MEN}-O_{MEN} $g(r)$ computed for the TBT:MEN system is slightly more intense than the BHT:MEN one, this feature nicely correlating with the redshift of the ν_{OH} band of MEN observed by FTIR spectroscopy (Figure 3a,b). This circumstance is corroborated by the comparison with liquid MEN, which has been simulated at 353 K and compared with the BHT:MEN eutectic at the same temperature. Also here, the superimposed H_{MEN}-O_{MEN} $g(r)$'s computed for the two systems show similar shapes (Figure 4c), but the integration of these functions up to the same cutoff at 2.87 Å provided coordination numbers of 0.32 for liquid MEN and 0.40 for the BHT:MEN. This result evidences that the MEN−MEN H-bond in the BHT:MEN mixture is even stronger than in the pure MEN compound, thus confirming the observed MEN > BHT:MEN > TBT:MEN trend of the ν_{OH} band wavenumber. Here, we have to make a comment about the fact that the FTIR ν_{OH} band of MEN exhibits an almost equal redshift interval passing from liquid MEN to the BHT:MEN eutectic, and from the latter one to the TBT:MEN eutectic (Figure 3a), indicating a similar increase in the H-bond strength among these systems. Differently, the H_{MEN}-O_{MEN} $g(r)$'s computed for the BHT:MEN and TBT:MEN eutectics are very similar to each other (Figure 4b), while the same distribution shows larger differences between the BHT:MEN eutectic and liquid MEN (Figure 4c). In this respect, it must be considered that, although being both correlated to the H-bond strength, the shift of the FTIR ν_{OH} band is connected with a transfer of electron density from the HBD to the HBA hydroxyl groups as a consequence of the H-bond formation, while the H_{MEN}-O_{MEN} $g(r)$ reflects the relative structural arrangement between a pair of atoms; therefore, different factors are expected to play a role in the two analyses. In addition, while the H_{MEN}-O_{MEN} $g(r)$'s computed for the BHT:MEN and TBT:MEN eutectics (Figure 4b) are relative to a temperature of 308 K, that for the liquid MEN has been compared with the BHT:MEN system at 353 K (Figure 4c), the MEN compound being solid at room temperature. The larger discrepancy between the H_{MEN}-O_{MEN} distributions in the latter case can be therefore attributed also to temperature effects. In this framework, the achievement of a similar trend concerning the strengthening of the H_{MEN}-O_{MEN} interaction, as obtained by these two different techniques, is a noteworthy result.

Hydrophobic Segregation and Global Structural Order. The FTIR and MD results show that almost no H-bonds are formed between the MEN and either the BHT or

https://doi.org/10.1021/acssuschemeng.2c00920
ACS Sustainable Chem. Eng. 2022, 10, 6337−6345

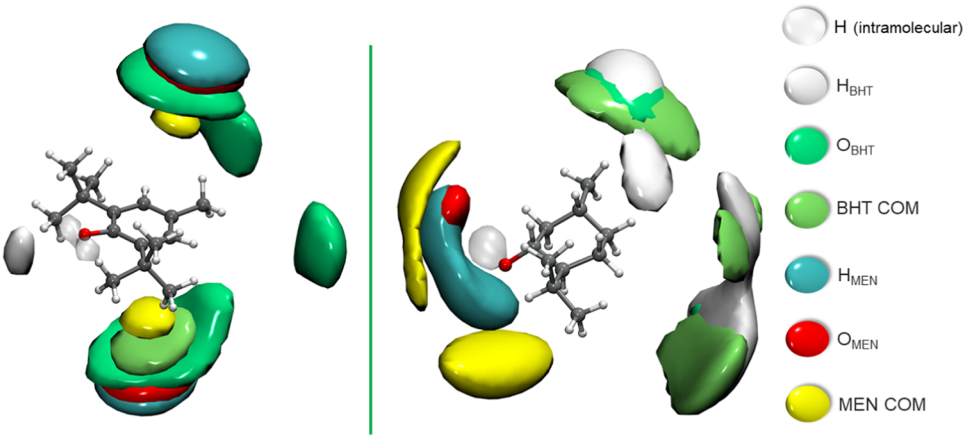

Figure 5. Spatial distribution functions (SDFs) around the BHT (left) and MEN (right) molecules calculated from the MD simulations of the BHT:MEN system. The functions have been computed with respect to an internal reference system that for both the BHT and MEN is integral to the carbon ring. The observed species are shown according to the color code reported on the right, while the atom names are employed with the nomenclature of Figure 1. The hydroxyl hydrogen atom of both molecules is represented by intramolecular SDFs. Isosurfaces have been drawn with the same density/maximum density ratio according to the following isovalues in nm^{-3}. For the SDFs around BHT: H_{BHT} (1.0), O_{BHT} (1.0), BHT COM (1.5), H_{MEN} (3.6), O_{MEN} (3.3), MEN COM (5.3); around MEN: H_{BHT} (0.9), O_{BHT} (1.0), BHT COM (1.1), H_{MEN} (8.4), O_{MEN} (9.5), and MEN COM (4.9). The same values have been employed for the SDFs computed for the TBT:MEN system (Figure S4).

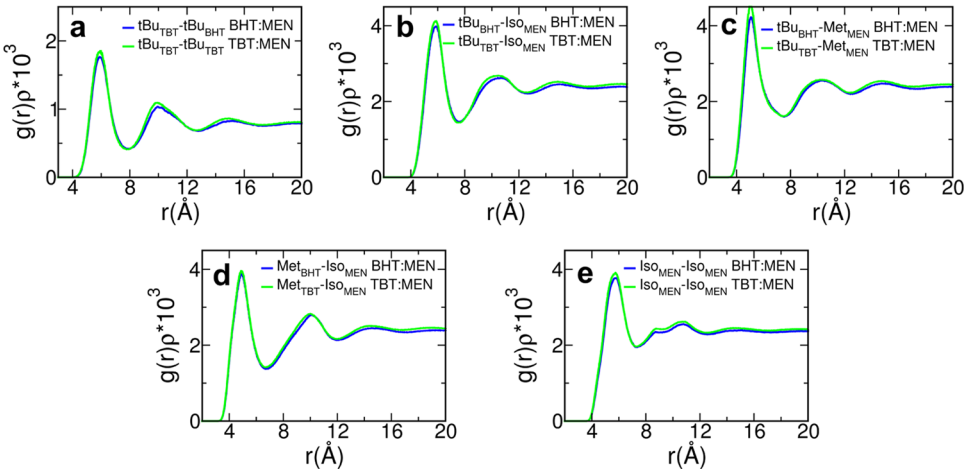

Figure 6. (a–e) Radial distribution functions multiplied by the numerical densities of the observed centers, $g(r)\rho$'s, calculated between the COMs of the alkyl functional groups of the components from the MD simulation of the BHT:MEN (blue lines) and TBT:MEN (green lines) systems. The group names are employed according to the nomenclature reported in Figure 1.

TBT components in the BHT:MEN and TBT:MEN mixtures. However, given that these compounds melt upon contact to provide liquid mixtures, this circumstance opens the question about what are the favorable interactions at the base of the eutectic formation and if a preferential structural arrangement is anyway discernible in solution. To unveil the three-dimensional arrangement of these compounds, spatial distribution functions (SDFs) for the single constituents have been computed from the MD simulation of the BHT:MEN and TBT:MEN systems. The obtained surfaces for the BHT:MEN eutectic are shown in Figure 5. In the SDFs computed around the BHT molecule, the first feature that draws attention is that almost no probability spots are found in the region of space close to the hydroxyl group, confirming its negligible involvement in the H-bond interactions. Conversely, the observed species are located close to the carbon body of BHT, in particular below and above the aromatic ring and next to the methyl group. On the other hand, the SDFs computed around the MEN component are split into two regions: the surfaces connected with the observed MEN molecules are localized around the hydroxyl group as a consequence of the H_{MEN}-O_{MEN} H-bond, while the SDFs belonging to the BHT molecules are found on the opposite side of MEN hydroxyl group, in the neighborhood of the isopropyl and methyl substituents. Such a result provides a picture of how the MEN molecules are disposed to expose to each other their hydrophilic part consisting in the hydroxyl groups and to promote the H-bond interactions. On the other hand, the incompatibility between the MEN and BHT constituents in terms of H-bonds formation turns into segregation of the BHT in the molecular regions of MEN that are far away from the hydroxyl moiety and closer to the alkyl groups. It is remarkable that the correspondent SDFs computed for the TBT:MEN system exhibit a similar picture (Figure S4).

To get more details about the relative arrangement of the hydrophobic parts of the MEN, BHT, and TBT molecules, the $g(r)$'s between the centers of mass (COMs) of their alkyl substituents have also been computed (Figure 6). As can be

https://doi.org/10.1021/acssuschemeng.2c00920
ACS Sustainable Chem. Eng. 2022, 10, 6337−6345

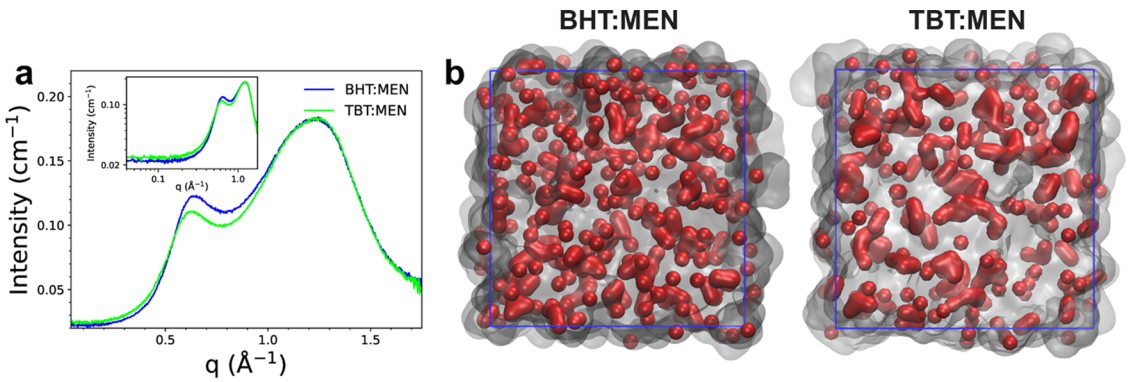

Figure 7. (a) Experimental SWAXS spectra collected on the BHT:MEN (blue line) and TBT:MEN (green line) eutectics. In the main figure, the data are shown in linear scale to highlight the WAXS peaks, while in the inset, they are plotted in double-logarithmic scale to emphasize the low-q region. (b) Snapshots taken from the final configuration of the MD simulations performed on the BHT:MEN and TBT:MEN systems. Oxygen atoms are visualized as red surfaces, while carbon and hydrogen atoms are shown in transparent gray. Box edges are highlighted by blue lines.

observed, all of the curves present well-defined first peaks showing a remarkable degree of structuration, as also shown by the relatively high coordination numbers listed in Table S2. Once again, the obtained functions are almost superimposable between the BHT:MEN and TBT:MEN systems, confirming the similar structural arrangement of the two eutectics. This result corroborates the picture of how the mixed components arrange themselves to expose their hydrophobic parts, given that no H-bonds can be established between the MEN and the BHT or TBT molecules. Note that it is difficult to say if the structured distribution observed between the alkyl chains is translated into a proper apolar−apolar interaction ruled by vdW forces. However, in the framework of the quest about the favorable interactions ruling the lowering of the MP of the mixtures, the obtained picture, together with the observation that no H-bonds can be established between MEN and BHT/TBT, suggests that these apolar−apolar attractions are the principal cause at the base of the BHT:MEN and TBT:MEN eutectics formation.

On a larger scale length, the effect of the observed structural arrangement on the intermediate-range order in solution can be assessed from the SWAXS spectra collected on both the BHT:MEN and TBT:MEN eutectics (Figure 7a). At first glance, the two scattering profiles look very similar, especially for what concerns the WAXS main peak occurring at 1.23 Å^{-1} for both systems. A diagnostic feature is the presence of a prepeak occurring at ≈0.63 Å^{-1}, corresponding to distances of ≈10.0 Å in the real space. Note that this prepeak is slightly shifted at higher q values for the BHT:MEN mixture with respect to the TBT:MEN one. For type V HDESs based on MEN with either thymol or carboxylic acids, the appearance of such a prepeak has been previously associated with the formation of heterogeneities induced by the established H-bonds in solution.[51,52] As a consequence, areas of higher electron density are produced and are segregated from regions of lower density consisting of the carbon bodies of the constituents, acting as molecular spacers. This feature originates from the fact that the steric exclusion between the carbon rings of the components prevents the formation of a continuous H-bond network, as it would be in H-bonded liquids with closer packing like water or methanol.[53] In our case, the only relevant H-bonds in solution are the MEN−MEN ones so that regions of higher electron density are formed by the hydroxyl groups of these molecules. However, the WAXS prepeak of the TBT:MEN eutectic is significantly less intense with respect to the BHT:MEN one. This result suggests that, even if the BHT molecules do not participate in the H-bond network, they are in any case embedded in a structural order contributing to the global electron density contrast by means of their hydroxyl groups. Such a picture can be appreciated from a qualitative point of view from the MD snapshots reported in Figure 7b, where the oxygen atoms contributing to the areas of higher electron density are depicted as red surfaces, while the carbon and hydrogen atoms are in gray. Here, it can be observed that the low-density areas in the BHT:MEN system are interspersed by red areas belonging to the oxygen atoms of the BHT, at variance with the TBT:MEN system. This evidence also provides an explanation for the occurrence of the BHT:MEN WAXS prepeak at slightly larger q values compared to the TBT:MEN one, therefore indicating on average shorter distances among the oxygen atoms. The formation of such intermediate-range organization in the studied eutectics, which makes them appear as ordered liquids, is remarkable, in particular, if we take into account the absence of a highly directional interaction like the H-bond between the components.

CONCLUSIONS

A detailed study of the BHT:MEN and TBT:MEN hydrophobic eutectics has been carried out with the main goal of understanding the structural arrangement in solution and the interactions ruling the eutectic formation. The two mixtures show great similarity in the measured DSC traces, highlighting that the hydroxyl group of the BHT component has little or no impact on the thermal behavior of the eutectic. The ATR-FTIR spectra collected on the mixtures and on the pure compounds evidence that almost no H-bonds are established between the BHT and the MEN components in the BHT:MEN eutectic. In addition, after mixing with the BHT, the MEN retains a degree of H-bonding that is slightly higher than in the pure compound. This trend is even more pronounced in the TBT:MEN eutectic, suggesting that the incompatibility between these constituents in terms of H-bond formation is translated into a hydrophobic segregation of the MEN molecules. The MD simulations confirm this picture and unambiguously show that the high steric hindrance suffered by the BHT hydroxyl group prevents the formation of H-bonds by this component. This is a quite surprising result, since these eutectics, and in particular DESs, are often indicated as extensively H-bonded liquids, where the high degree of H-

https://doi.org/10.1021/acssuschemeng.2c00920
ACS Sustainable Chem. Eng. 2022, 10, 6337−6345

bonding between the constituents allows the lowering of the MP of the mixture. The obtained three-dimensional spatial arrangement among the components indicates that, with the exception of the MEN−MEN case, each species is located in regions of space far from the hydroxyl groups and close to the carbon bodies of the other constituents. The highly ordered distribution observed among the alkyl functional groups suggests that apolar−apolar attractions between the constituents might be at the base of the eutectic formation. This structural arrangement results in the appearance of a WAXS prepeak in the collected SWAXS data, which is indicative of the establishment of an intermediate-range order in solution. The considerations reported here have the impact of deepening the knowledge about hydrophobic eutectics and are of potential interest for the employment of these innovative solvents in any application, while also challenging the fundamental definition of DESs.

■ ASSOCIATED CONTENT

Supporting Information

The Supporting Information is available free of charge at https://pubs.acs.org/doi/10.1021/acssuschemeng.2c00920.

Additional details of the simulated MD systems, additional DSC traces, and MD analyses (PDF)

■ AUTHOR INFORMATION

Corresponding Authors

Matteo Busato − *Department of Chemistry, University of Rome "La Sapienza", 00185 Rome, Italy;* orcid.org/0000-0002-9450-0481; Email: matteo.busato@uniroma1.it

Paola D'Angelo − *Department of Chemistry, University of Rome "La Sapienza", 00185 Rome, Italy;* orcid.org/0000-0001-5015-8410; Email: p.dangelo@uniroma1it

Authors

Giorgia Mannucci − *Department of Chemistry, University of Rome "La Sapienza", 00185 Rome, Italy*

Valerio Di Lisio − *Department of Chemistry, University of Rome "La Sapienza", 00185 Rome, Italy*

Andrea Martinelli − *Department of Chemistry, University of Rome "La Sapienza", 00185 Rome, Italy;* orcid.org/0000-0002-6401-9988

Alessandra Del Giudice − *Department of Chemistry, University of Rome "La Sapienza", 00185 Rome, Italy;* orcid.org/0000-0002-1916-8300

Alessandro Tofoni − *Department of Chemistry, University of Rome "La Sapienza", 00185 Rome, Italy;* orcid.org/0000-0003-1935-4063

Chiara Dal Bosco − *Department of Chemistry, University of Rome "La Sapienza", 00185 Rome, Italy*

Valentina Migliorati − *Department of Chemistry, University of Rome "La Sapienza", 00185 Rome, Italy;* orcid.org/0000-0003-4733-6188

Alessandra Gentili − *Department of Chemistry, University of Rome "La Sapienza", 00185 Rome, Italy;* orcid.org/0000-0002-9541-3857

Complete contact information is available at: https://pubs.acs.org/10.1021/acssuschemeng.2c00920

Notes

The authors declare no competing financial interest.

■ ACKNOWLEDGMENTS

Part of the calculations was performed on the Marconi100 system of the CINECA supercomputing center (grant IsC88_MDES2021). The authors acknowledge financial support from the Italian Ministry of University and Research (MIUR) through Grant PRIN 2017, 2017KKP5ZR, MOSCA-To, and from the University of Rome "La Sapienza" Grant RG11916B702B43B9. The Sapienza Research Infrastructure is acknowledged for the SWAXS measurements at SAXSLab Sapienza.

■ REFERENCES

(1) Abbott, A. P.; Capper, G.; Davies, D. L.; Rasheed, R. K.; Tambyrajah, V. Novel solvent properties of choline chloride/urea mixtures. *Chem. Commun.* **2003**, 70−71.

(2) Martins, M. A. R.; Pinho, S.; Coutinho, J. Insights into the Nature of Eutectic and Deep Eutectic Mixtures. *J. Solution Chem.* **2019**, *48*, 962−982.

(3) Migliorati, V.; Sessa, F.; D'Angelo, P. Deep eutectic solvents: A structural point of view on the role of the cation. *Chem. Phys. Lett. X* **2019**, *737*, No. 100001.

(4) Busato, M.; Migliorati, V.; Del Giudice, A.; Di Lisio, V.; Tomai, P.; Gentili, A.; D'Angelo, P. Anatomy of a deep eutectic solvent: structural properties of choline chloride:sesamol 1:3 compared to reline. *Phys. Chem. Chem. Phys.* **2021**, *23*, 11746−11754.

(5) Busato, M.; Di Lisio, V.; Del Giudice, A.; Tomai, P.; Migliorati, V.; Galantini, L.; Gentili, A.; Martinelli, A.; D'Angelo, P. Transition from molecular- to nano-scale segregation in a deep eutectic solvent - water mixture. *J. Mol. Liq.* **2021**, *331*, 115747.

(6) Busato, M.; Del Giudice, A.; Di Lisio, V.; Tomai, P.; Migliorati, V.; Gentili, A.; Martinelli, A.; D'Angelo, P. Fate of a Deep Eutectic Solvent upon Cosolvent Addition: Choline Chloride-Sesamol 1:3 Mixtures with Methanol. *ACS Sustainable Chem. Eng.* **2021**, *9*, 12252−12261.

(7) Ashworth, C. R.; Matthews, R. P.; Welton, T.; Hunt, P. A. Doubly ionic hydrogen bond interactions within the choline chloride-urea deep eutectic solvent. *Phys. Chem. Chem. Phys.* **2016**, *18*, 18145−18160.

(8) Perkins, S. L.; Painter, P.; Colina, C. M. Molecular Dynamic Simulations and Vibrational Analysis of an Ionic Liquid Analogue. *J. Phys. Chem. B* **2013**, *117*, 10250−10260.

(9) Sun, H.; Li, Y.; Wu, X.; Li, G. Theoretical study on the structures and properties of mixtures of urea and choline chloride. *J. Mol. Model.* **2013**, *19*, 2433−2441.

(10) Francisco, M.; van den Bruinhorst, A.; Kroon, M. C. Low-Transition-Temperature Mixtures (LTTMs): A New Generation of Designer Solvents. *Angew. Chem., Int. Ed.* **2013**, *52*, 3074−3085.

(11) Smith, E. L.; Abbott, A. P.; Ryder, K. S. Deep Eutectic Solvents (DESs) and Their Applications. *Chem. Rev.* **2014**, *114*, 11060−11082.

(12) Durand, E.; Lecomte, J.; Villeneuve, P. From green chemistry to nature: The versatile role of low transition temperature mixtures. *Biochimie* **2016**, *120*, 119−123.

(13) Abranches, D. O.; Martins, M. A. R.; Silva, L. P.; Schaeffer, N.; Pinho, S. P.; Coutinho, J. A. P. Phenolic hydrogen bond donors in the formation of non-ionic deep eutectic solvents: the quest for type V DES. *Chem. Commun.* **2019**, *55*, 10253−10256.

(14) van Osch, D. J.; Zubeir, L. F.; van den Bruinhorst, A.; Rocha, M. A.; Kroon, M. C. Hydrophobic deep eutectic solvents as water-immiscible extractants. *Green Chem.* **2015**, *17*, 4518−4521.

(15) Ribeiro, B. D.; Florindo, C.; Iff, L. C.; Coelho, M. A. Z.; Marrucho, I. M. Menthol-based Eutectic Mixtures: Hydrophobic Low Viscosity Solvents. *ACS Sustainable Chem. Eng.* **2015**, *3*, 2469−2477.

(16) van Osch, D. J. G. P.; Dietz, C. H. J. T.; Warrag, S. E. E.; Kroon, M. C. The Curious Case of Hydrophobic Deep Eutectic Solvents: A Story on the Discovery, Design, and Applications. *ACS Sustainable Chem. Eng.* **2020**, *8*, 10591−10612.

(17) Martins, M. A. R.; Silva, L. P.; Schaeffer, N.; Abranches, D. O.; Maximo, G. J.; Pinho, S. P.; Coutinho, J. A. P. Greener Terpene-Terpene Eutectic Mixtures as Hydrophobic Solvents. *ACS Sustainable Chem. Eng.* **2019**, *7*, 17414−17423.
(18) Dal Bosco, C.; Mariani, F.; Gentili, A. Hydrophobic Eutectic Solvent-Based Dispersive Liquid-Liquid Microextraction Applied to the Analysis of Pesticides in Wine. *Molecules* **2022**, *27*, No. 908.
(19) Tang, W.; Dai, Y.; Row, K. Evaluation of fatty acid/alcohol-based hydrophobic deep eutectic solvents as media for extracting antibiotics from environmental water. *Anal. Bioanal. Chem.* **2018**, *410*, 7325−7336.
(20) Schaeffer, N.; Conceição, J. H. F.; Martins, M. A. R.; Neves, M. C.; Pérez-Sánchez, G.; Gomes, J. R. B.; Papaiconomou, N.; Coutinho, J. A. P. Non-ionic hydrophobic eutectics - versatile solvents for tailored metal separation and valorisation. *Green Chem.* **2020**, *22*, 2810−2820.
(21) Zante, G.; Boltoeva, M. Review on Hydrometallurgical Recovery of Metals with Deep Eutectic Solvents. *Sustainable Chem.* **2020**, *1*, 238−255.
(22) Schaeffer, N.; Martins, M. A. R.; Neves, C. M. S. S.; Pinho, S. P.; Coutinho, J. A. P. Sustainable hydrophobic terpene-based eutectic solvents for the extraction and separation of metals. *Chem. Commun.* **2018**, *54*, 8104−8107.
(23) van Osch, D. J. G. P.; Parmentier, D.; Dietz, C. H. J. T.; van den Bruinhorst, A.; Tuinier, R.; Kroon, M. C. Removal of alkali and transition metal ions from water with hydrophobic deep eutectic solvents. *Chem. Commun.* **2016**, *52*, 11987−11990.
(24) Murakami, Y.; Das, S. K.; Himuro, Y.; Maeda, S. Triplet-sensitized photon upconversion in deep eutectic solvents. *Phys. Chem. Chem. Phys.* **2017**, *19*, 30603−30615.
(25) Zubeir, L. F.; van Osch, D. J. G. P.; Rocha, M. A. A.; Banat, F.; Kroon, M. C. Carbon Dioxide Solubilities in Decanoic Acid-Based Hydrophobic Deep Eutectic Solvents. *J. Chem. Eng. Data* **2018**, *63*, 913−919.
(26) Li, T.; Song, Y.; Xu, J.; Fan, J. A hydrophobic deep eutectic solvent mediated sol-gel coating of solid phase microextraction fiber for determination of toluene, ethylbenzene and o-xylene in water coupled with GC-FID. *Talanta* **2019**, *195*, 298−305.
(27) Milker, S.; Pätzold, M.; Bloh, J.; Holtmann, D. Comparison of deep eutectic solvents and solvent-free reaction conditions for aldol production. *Mol. Catal.* **2019**, *466*, 70−74.
(28) Dal Bosco, C.; Di Lisio, V.; D'Angelo, P.; Gentili, A. Hydrophobic Eutectic Solvent with Antioxidant Properties: Application for the Dispersive Liquid-Liquid Microextraction of Fat-Soluble Micronutrients from Fruit Juices. *ACS Sustainable Chem. Eng.* **2021**, *9*, 8170−8178.
(29) Yehye, W. A.; Rahman, N. A.; Ariffin, A.; AbdHamid, S. B.; Alhadi, A. A.; Kadir, F. A.; Yaeghoobi, M. Understanding the chemistry behind the antioxidant activities ofbutylated hydroxytoluene (BHT): A review. *Eur. J. Med. Chem.* **2015**, *101*, 295−312.
(30) Jorgensen, W. L.; Maxwell, D. S.; Tirado-Rives, J. Development and Testing of the OPLS All-Atom Force Field on Conformational Energetics and Properties of Organic Liquids. *J. Am. Chem. Soc.* **1996**, *118*, 11225−11236.
(31) Jasik, M.; Szefczyk, B. Parameterization and optimization of the menthol force field for molecular dynamics simulations. *J. Mol. Model.* **2016**, *22*, No. 234.
(32) Darden, T.; York, D.; Pedersen, L. Particle mesh Ewald: An Nlog(N) method for Ewald sums in large systems. *J. Chem. Phys.* **1993**, *98*, 10089−10092.
(33) Essmann, U.; Perera, L.; Berkowitz, M. L.; Darden, T.; Lee, H.; Pedersen, L. G. A smooth particle mesh Ewald method. *J. Chem. Phys.* **1995**, *103*, 8577−8593.
(34) Martínez, L.; Andrade, R.; Birgin, E. G.; Martínez, J. M. PACKMOL: A package for building initial configurations for molecular dynamics simulations. *J. Comput. Chem.* **2009**, *30*, 2157−2164.
(35) Busato, M.; Lapi, A.; D'Angelo, P.; Melchior, A. Coordination of the Co^{2+} and Ni^{2+} Ions in Tf_2N^- Based Ionic Liquids: A Combined X-ray Absorption and Molecular Dynamics Study. *J. Phys. Chem. B* **2021**, *125*, 6639−6648.
(36) Busato, M.; D'Angelo, P.; Lapi, A.; Tolazzi, M.; Melchior, A. Solvation of Co^{2+} ion in 1-butyl-3-methylimidazolium bis-(trifluoromethylsulfonyl)imide ionic liquid: A molecular dynamics and X-ray absorption study. *J. Mol. Liq.* **2020**, *299*, No. 112120.
(37) Sessa, F.; Migliorati, V.; Serva, A.; Lapi, A.; Aquilanti, G.; Mancini, G.; D'Angelo, P. On the coordination of Zn^{2+} ion in $Tf2N^-$ based ionic liquids: structural and dynamic properties depending on the nature of the organic cation. *Phys. Chem. Chem. Phys.* **2018**, *20*, 2662−2675.
(38) Busato, M.; D'Angelo, P.; Melchior, A. Solvation of Zn^{2+} ion in 1-alkyl-3-methylimidazolium bis(trifluoromethylsulfonyl)imide ionic liquids: a molecular dynamics and X-ray absorption study. *Phys. Chem. Chem. Phys.* **2019**, *21*, 6958−6969.
(39) Migliorati, V.; Gibiino, A.; Lapi, A.; Busato, M.; D'Angelo, P. On the Coordination Chemistry of the lanthanum(III) Nitrate Salt in EAN/MeOH Mixtures. *Inorg. Chem.* **2021**, *60*, 10674−10685.
(40) Abbott, A.; Abe, H.; Aldous, L.; et al. Phase behaviour and thermodynamics: general discussion. *Faraday Discuss.* **2018**, *206*, 113−139.
(41) Hess, B.; Bekker, H.; Berendsen, H. J. C.; Fraaije, J. G. E. M. LINCS: A linear constraint solver for molecular simulations. *J. Comput. Chem.* **1997**, *18*, 1463−1472.
(42) Ding, J.; Xu, M.; Guan, P. F.; Deng, S. W.; Cheng, Y. Q.; Ma, E. Temperature effects on atomic pair distribution functions of melts. *J. Chem. Phys.* **2014**, *140*, No. 064501.
(43) Popov, G.; Kolarov, K.; Veltschev, C.; Manolov, K. R. Physical characteristics of the main components of Bulgarian essential oils. *Monatsh. Chem.* **1977**, *108*, 159−161.
(44) Abraham, M. J.; Murtola, T.; Schulz, R.; Páll, S.; Smith, J. C.; Hess, B.; Lindahl, E. GROMACS: High performance molecular simulations through multi-level parallelism from laptops to supercomputers. *SoftwareX* **2015**, *1−2*, 19−25.
(45) Humphrey, W.; Dalke, A.; Schulten, K. VMD: Visual molecular dynamics. *J. Mol. Graph.* **1996**, *14*, 33−38.
(46) Brehm, M.; Kirchner, B. TRAVIS - A free analyzer and visualizer for monte carlo and molecular dynamics trajectories. *J. Chem. Inf. Model.* **2011**, *51*, 2007−2023.
(47) Sztucki, M.; Narayanan, T. Development of an ultra-small-angle X-ray scattering instrument for probing the microstructure and the dynamics of soft matter. *J. Appl. Crystallogr.* **2007**, *40*, s459−s462.
(48) Bradley, J.-C.; Williams, A.; Lang, A. *Jean-Claude Bradley Open Melting Point Dataset*, 2014, DOI: 10.6084/m9.figshare.1031637.v.
(49) Ojha, D.; Karhan, K.; Kühne, T. On the Hydrogen Bond Strength and Vibrational Spectroscopy of Liquid Water. *Sci. Rep.* **2018**, *8*, No. 16888.
(50) Herschlag, D.; Pinney, M. M. Hydrogen Bonds: Simple after All? *Biochem* **2018**, *57*, 3338−3352.
(51) Malik, A.; Kashyap, H. K. Heterogeneity in hydrophobic deep eutectic solvents: SAXS prepeak and local environments. *Phys. Chem. Chem. Phys.* **2021**, *23*, 3915−3924.
(52) Schaeffer, N.; Abranches, D. O.; Silva, L. P.; Martins, M. A.; Carvalho, P. J.; Russina, O.; Triolo, A.; Paccou, L.; Guinet, Y.; Hedoux, A.; Coutinho, J. A. Non-Ideality in Thymol + Menthol Type V Deep Eutectic Solvents. ACS Sustain. *Chem. Eng.* **2021**, *9*, 2203−2211.
(53) Morineau, D.; Alba-Simionesco, C.; Bellissent-Funel, M.-C.; Lauthié, M.-F. Experimental indication of structural heterogeneities in fragile hydrogen-bonded liquids. *Europhys. Lett.* **1998**, *43*, 195−200.